Synthesis and electrocatalytic properties of a dinuclear copper(II) complex for generating hydrogen from acetic acid or water

Ting Fang, Wei Li, Shu-Zhong Zhan & Xiao-Lan Wei

Taylor & Francis
Taylor & Francis Group

Synthesis and electrocatalytic properties of a dinuclear copper(II) complex for generating hydrogen from acetic acid or water

TING FANG†, WEI LI‡, SHU-ZHONG ZHAN*† and XIAO-LAN WEI†

†College of Chemistry and Chemical Engineering, South China University of Technology, Guangzhou, China
‡School of Chemistry and Environmental Science, Guizhou Minzu University, Guiyang, China
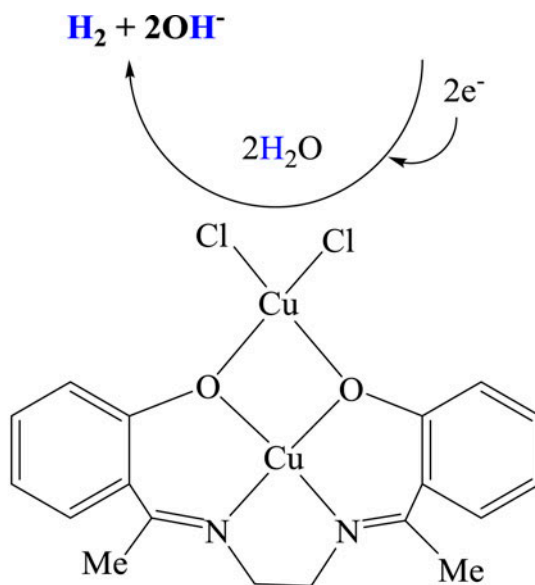
The reaction of $CuCl_2 \cdot 2H_2O$ and a tetradentate amine phenol ligand affords a dinuclear Cu(II) complex, **1**, a new molecular electrocatalyst, whose structure has been determined by X-ray crystallography. Electrochemical studies show that **1** can efficiently produce hydrogen from acetic acid with a turnover frequency (TOF) of 50.1 (in DMF) or from water with a TOF of 104.3 (pH 7.0) moles of hydrogen per mole of catalyst per hour.

Keywords: Copper(II)-complex; Molecular electro-catalyst; Water reduction; Hydrogen evolution

*Corresponding author. Email: shzhzhan@scut.edu.cn

1. Introduction

The ability to store and recover secure, clean, and sustainable energy is arguably the most important scientific and technical challenge facing humanity in the twenty-first century. Chemical fuels are ideal in this context since chemical bonds have high energy density; hydrogen has attracted considerable attention as an alternative chemical fuel. On a mid- to long-term basis, it is urgent to provide an appealing approach toward generating and storing hydrogen [1–3]. In nature, hydrogenase enzymes [4, 5] can efficiently catalyze both the production and oxidation of hydrogen using earth-abundant metals (nickel and iron). However, enzymes are difficult to obtain in sufficient amounts to adapt for commercial applications and their stability is often limited outside of their native environment [4–7]. Electrolysis of water is the simplest way to produce hydrogen. To increase the reaction rate and lower the overpotential, it is necessary to use an efficient hydrogen evolution reaction (HER) electrocatalyst. These considerations have led to development of molecular catalysts employing more abundant metals, and several complexes that contain nickel [8–10], cobalt [11–13], iron [14, 15], and molybdenum [16], have been developed as electrocatalysts for reduction of water to form H_2. Although there has been significant progress in designing molecular catalysts for H_2 evolution, the search for robust and highly active catalysts that can operate in purely aqueous solution still remains a challenge [11]. In designing a model featuring both water oxidation and reduction functionality, we sought a synthetic cofactor with the following properties: (1) the metal center coordination geometry is planar; (2) mild redox couple closer to the H_2/H^+ couple, in the range −0.70 to −1.45 V *versus* SHE; (3) chemical inertness, so that reactions would be localized at the metal centers. In general, copper complexes are employed as electrocatalysts for water oxidation [17, 18]. Here, we present the synthesis, structure and properties of a new dinuclear copper(II) complex, **1**, that can catalyze hydrogen evolution from acetic acid or water.

2. Experimental

2.1. *Materials and physical measurements*

All commercially available reagents were used as received without purification. UV–vis spectrum was measured on a Hitachi U-3010 spectrometer. Cyclic voltammograms were obtained on a CHI-660E electrochemical analyzer under oxygen-free conditions using a three-electrode cell in which a glassy carbon electrode gas chromatograph (GC), 1 mm in diameter, was the working electrode, a saturated $Ag/AgNO_3$ electrode was the reference electrode, and platinum wire was the auxiliary electrode. A ferrocenium/ferrocene couple was used as an internal standard and $E_{1/2}$ of the ferrocenium/ferrocene ($FeCP_2^{+/0}$) couple under the experimental condition was 0.47 V. 0.1 M [(*n*-Bu)$_4$ N]ClO$_4$ was used as the supporting electrolyte. Acetic acid was added by syringe. Controlled-potential electrolysis (CPE) in DMF was conducted using an air-tight glass double compartment cell separated by a glass frit. The working compartment was fitted with a glassy carbon plate and an $Ag/AgNO_3$ reference electrode. The auxiliary compartment was fitted with a Pt gauze electrode. The working compartment was filled with 50 mL of 33.3 mM acetic acid in a 0.1 M [(*n*-Bu$_4$ N)]ClO$_4$ DMF solution, while the auxiliary compartment was filled with 35 mL of 0.1 M [(*n*-Bu$_4$ N)]ClO$_4$ DMF solution, resulting in equal solution levels in both

compartments. Both compartments were sparged for 60 min with N_2 and cyclic voltammograms were recorded as controls. Complex **1** (4.41 μM) was then added and a cyclic voltammogram was recorded. CPE in aqueous media was also conducted using an air-tight glass double compartment cell separated by a glass frit. The working compartment was fitted with a glassy carbon plate and a Ag/AgCl reference electrode. The auxiliary compartment was fitted with a Pt gauze electrode. The working compartment was filled with 50 mL of 0.25 M phosphate buffer solution ($CH_3CN : H_2O = 2 : 3$ as solvent) at different pH values containing 0.1 M KCl of the supporting electrolyte, while the auxiliary compartment was filled with 35 mL dihydrogen phosphate buffer solution. Both compartments were sparged for 60 min with N_2 and cyclic voltammograms were recorded as controls. Complex **1** (2.20 μM) was then added and a cyclic voltammogram was recorded. After electrolysis under a nitrogen atmosphere, a 0.5 mL aliquot of the headspace was removed and replaced with 0.5 mL of CH_4. A sample of the headspace was injected into the GC. GC experiments were carried out with an Agilent Technologies 7890A gas chromatography instrument.

2.2. Synthesis of 1

To a solution of 4 mM of 2-hydroxyacetophenone in 30 mL of methanol was added a solution of 2 mM of ethylenediamine in 10 mL of methanol. The mixture was heated at reflux for 3 h, giving a yellow powder. To the yellow mixture was added 4 mM $CuCl_2\cdot 2H_2O$ with stirring; the color of the solution changed from yellow to violet. Single crystals were obtained from the filtrate which was allowed to stand at room temperature for several days, collected by filtration, and dried *in vacuo* (0.506 g, 50.2%). The elemental analysis results (found: C, 43.67; H, 3.67; N, 5.71. $C_{18}H_{18}Cl_2Cu_2N_2O_2$ requires C, 43.87; H, 3.66; N, 5.69) were in agreement with the formula of the sample used for X-ray analysis.

Table 1. Crystallographic data for **1**.

Empirical formula	$C_{18}H_{18}Cl_2Cu_2N_2O_2$
Formula weight	492.32
λ (Å)	0.71073
Crystal system	Monoclinic
Space group	*P2(1)/n*
a (Å)	7.6557(19)
b (Å)	18.573(5)
c (Å)	13.117(3)
α (°)	90
β (°)	94.392(3)
γ (°)	90
V (Å^3)	1859.6(8)
Z	4
Dc/Mgm^{-3}	1.758
F (000)	992
θ range for data collection	2.69–25.50°
Reflections collected/unique	12,279/3406
Max. and min. transmission	0.6629 and 0.4467
Data/restraints/parameters	3406/0/237
Goodness-of-fit on F^2	1.055
Final R indices [$I > 2\sigma(I)$]	$R_1 = 0.0588$, $wR_2 = 0.1608$
R indices (all data)	$R_1 = 0.0702$, $wR_2 = 0.1696$

2.3. Crystal structure determination

The X-ray analysis of **1** was carried out with a Bruker SMART CCD area detector using graphite monochromated Mo-Kα radiation ($\lambda = 0.71073$ Å) at room temperature. All empirical absorption corrections were applied by using SADABS [19]. The structure was solved using direct methods and the corresponding non-hydrogen atoms are refined anisotropically. All hydrogens of the ligands were placed in calculated positions with fixed isotropic thermal parameters and included in the structure factor calculations in the final stage of full-matrix least-squares refinement. All calculations were performed using the SHELXTL computer program [20]. Crystallographic data for **1** are given in table 1 and selected bond lengths in table 2.

Table 2.   Selected bond distances (Å) and angles (°) for **1**.

Bond distances (Å)			
Cu(1)–O(2)	1.886(4)	Cu(1)–N(1)	1.903(4)
Cu(1)–O(1)	1.908(4)	Cu(1)–N(2)	1.912(4)
Cu(1)–Cu(2)	3.0128(11)	Cu(2)–O(2)	1.951(4)
Cu(2)–O(1)	2.097(4)	Cu(2)–Cl(2)	2.1903(19)
Cu(2)–Cl(1)	2.1925(17)		
Bond angles (°)			
O(2)–Cu(1)–N(1)	176.38(18)	O(2)–Cu(1)–O(1)	81.60(16)
N(1)–Cu(1)–O(1)	94.96(18)	O(2)–Cu(1)–N(2)	93.36(18)
N(1)–Cu(1)–N(2)	90.05(19)	O(1)–Cu(1)–N(2)	174.76(17)
O(2)–Cu(1)–Cu(2)	39.04(12)	N(1)–Cu(1)–Cu(2)	137.36(14)
O(1)–Cu(1)–Cu(2)	43.63(11)	N(2)–Cu(1)–Cu(2)	131.15(14)
O(2)–Cu(2)–O(1)	75.45(15)	O(2)–Cu(2)–Cl(2)	100.25(15)
O(1)–Cu(2)–Cl(2)	132.43(13)	O(2)–Cu(2)–Cl(1)	139.81(16)
O(1)–Cu(2)–Cl(1)	106.72(11)	Cl(2)–Cu(2)–Cl(1)	105.68(7)
O(2)–Cu(2)–Cu(1)	37.51(11)	O(1)–Cu(2)–Cu(1)	38.90(10)
Cl(2)–Cu(2)–Cu(1)	116.50(6)	Cl(1)–Cu(2)–Cu(1)	137.56(5)
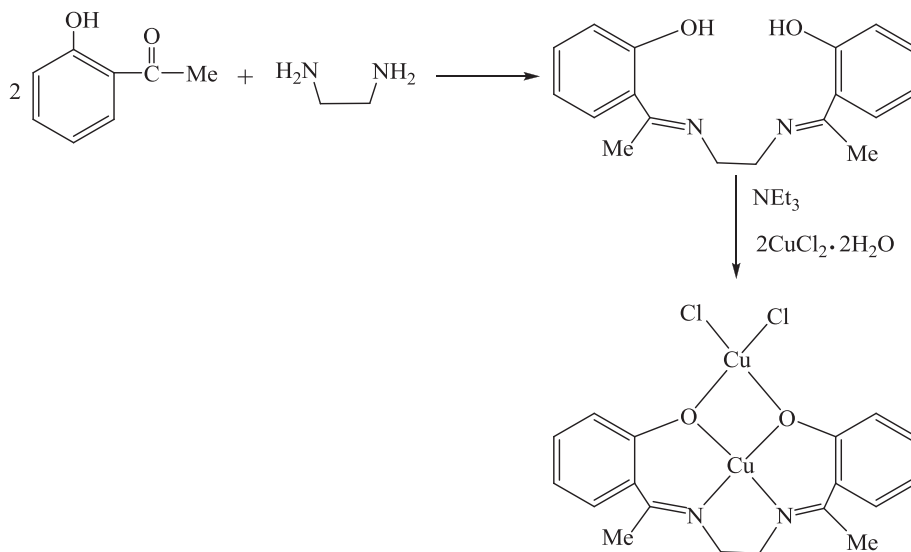
Scheme 1.   Schematic representation of the synthesis of **1**.

3. Results and discussion

3.1. *Structure analysis*

The reaction of $CuCl_2 \cdot 2H_2O$ and the tetradentate amine phenol ligand at one molar ratio set of 2 : 1 in the presence of triethylamine provides a dinuclear Cu(II) complex, **1** (scheme 1) (yield = 50%), which is air stable in the solid and soluble in DMF, CH_2Cl_2, and CH_3CN.

As shown in figure 1, two copper(II) ions are triply bridged by the phenolic oxygens, O1 and O2. The distance of Cu(1) and Cu(2) is 3.0128(11) Å, which is shorter than those of
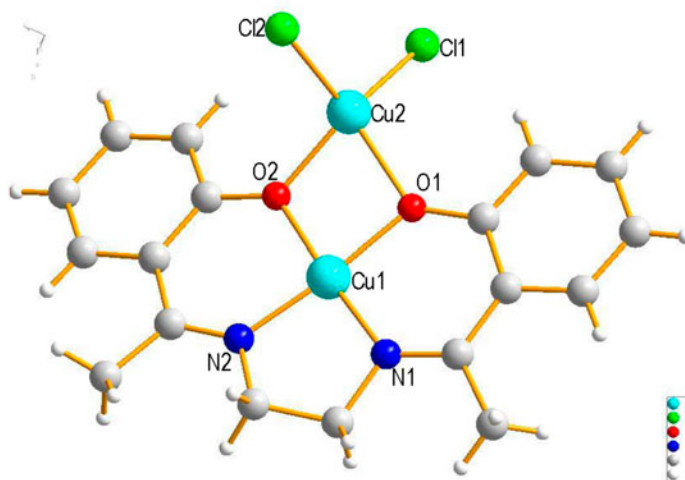
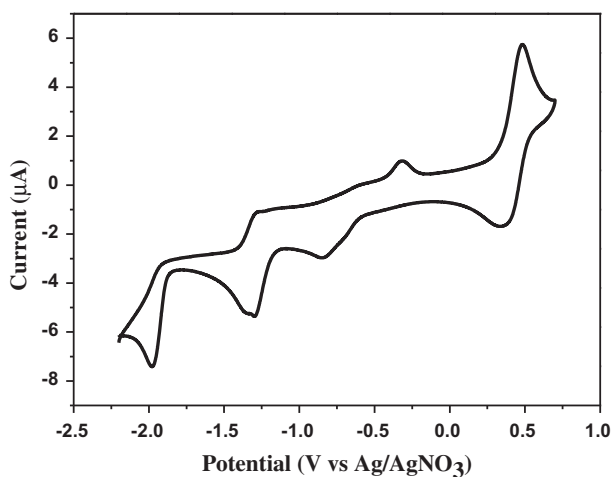

Figure 1.   Molecular structure of **1**.

Figure 2.   Cyclic voltammogram of **1** in 0.1 M of [n-Bu$_4$ N]ClO$_4$ DMF solution at a glassy carbon electrode and a scan rate of 100 mV s^{-1}. Ferrocene is the internal standard.

the reported carboxylate-bridged copper(II) complexes (from 3.1032(10) to 3.1716(12) Å) [21, 22]. Two Cu(II) ions are put in different environments. Cu(1) is coordinated by two amines and two phenolates from the amine-phenolate ligand in a slightly distorted square-planar coordination geometry. The average Cu–O and Cu–N distances are 1.897(4) and 1.9075(4) Å, respectively. These distances are in the range of those of conventional Schiff base copper (II) complexes of square-planar coordination [23–25].

Cu(2) has a distorted tetrahedral coordination geometry and is linked by two phenolate oxygens from the imine-phenolate ligand and two Cl ions. The Cu–Cl bond lengths are 2.1903(19) – 2.1925(17) Å. The average distances between Cu(2) and O of the Schiff base ligand is 2.024(4) Å, longer than that for Cu(1). The Cu(1)–O(1)–Cu(2) and Cu(1)–O(2)–Cu(2) bridging angles are 97.47(15) and 103.45(18)°, respectively. The bridging Cu(1),
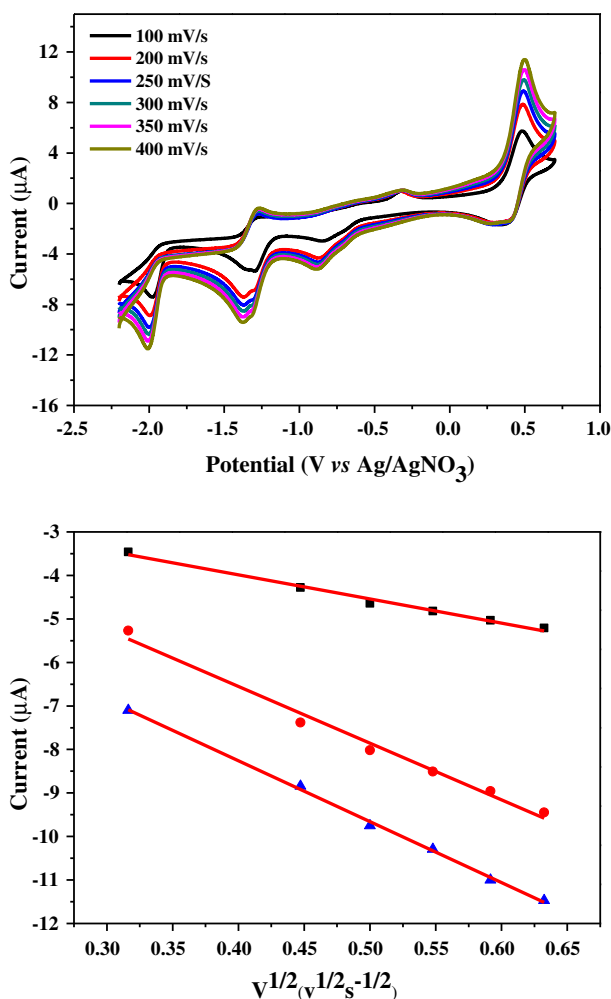

Figure 3.   Scan rate dependence of precatalytic waves for a 1.69 mM solution of **1** (0.1 M [*n*-Bu$_4$ N]ClO$_4$) at scan rates from 100 to 400 mV s^{-1}.

O(1), Cu(2), and O(2) is planar. The torsion angle N(1)–Cu(1)–O(2)–Cu(2) (−179.4(3)°) is the same as that for N(2)–Cu(1)–O(1)–Cu(2).

3.2. *Electronic spectrum*

The spectrum was recorded in CH_2Cl_2, with main features at 361 nm ($\varepsilon = 9800$) and 557 nm ($\varepsilon = 205$) (figure S1, see online supplemental material at http://dx.doi.org/10.1080/00958972.2014.998657). The shoulder observed at 361 nm corresponds to an LMCT
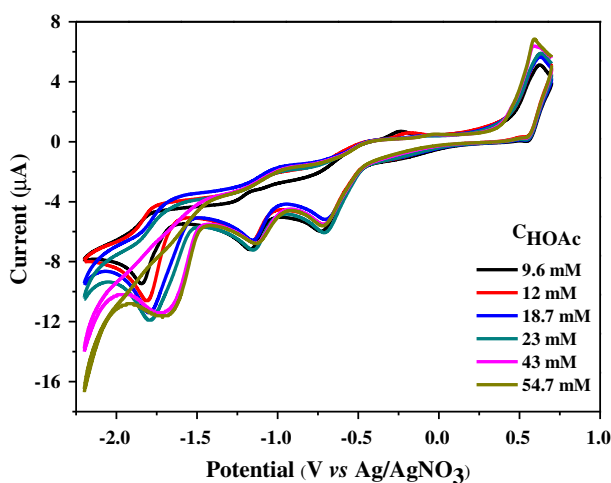

Figure 4. Cyclic voltammograms of a 1.69 mM solution of **1** with varying concentrations of acetic acid in DMF. Conditions: rt, 0.1 M [*n*-Bu$_4$ N]ClO$_4$ as supporting electrolyte, scan rate: 100 mV s^{-1}, GC working electrode (1 mm diameter), Pt counter electrode, Ag/AgNO$_3$ reference electrode, Fc internal standard.
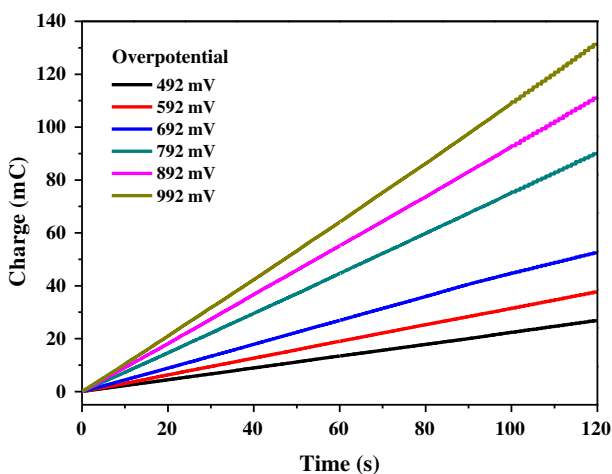

Figure 5. Charge buildup *vs.* time from electrolysis of a 8.1 μM **1** in DMF (0.1 M [*n*-Bu$_4$ N]ClO$_4$) under various overpotentials. All data have been deducted blank.

transition between the bridging phenoxo and copper ions. The band observed at 557 nm is characteristic of Cu(II) d–d transitions. Similar UV–visible features have been observed for several related (μ-phenoxo) dicopper(II) complexes [26, 27].

3.3. *Cyclic voltammetry studies*

Cyclic voltammogram of **1** in DMF was measured at a glassy carbon electrode (1 mm diameter) in the presence of 0.1 M [*n*-Bu$_4$ N]ClO$_4$ as supporting electrolyte. All potentials in this study were given *versus* the FeCp$_2$$^{+/0}$ couple internal standard. As shown in figure 2, cyclic voltammogram of **1** exhibits one quasi-reversible wave at −0.74 V and two reversible couples at −1.30 and −1.98 V *versus* Ag/AgNO$_3$. We assign the reversible couples to the metal-centered Cu$_2$$^{IV/III}$, Cu$_2$$^{III/II}$, and Cu$_2$$^{II/I}$ processes, respectively, which are different from those of the distorted square pyramidal copper(II) complex ($E_{1/2}$ = 0.087 and −0.125 V *versus* Ag/AgCl) [21]. As observed in figure 3, the current responses of the redox events both at −0.74, −1.30, and −1.98 V show linear dependence on the square root of the scan rate, which is indicative of a diffusion-controlled process, with the electrochemically active species freely diffusing in the solution. Such distinctive potential prompts possible usage of this complex as an electrocatalyst for HER.

3.4. *Catalytic hydrogen evolution in DMF*

To determine possible electrocatalytic activity of this complex, cyclic voltammograms of **1** were recorded in the presence of acetic acid. Figure 4 shows a systematic increase in i_{cat} observed near −1.37 V with increasing acid concentration from 9.6 to 54.7 mM. This rise in current can be attributed to catalytic generation of H$_2$ from acetic acid, with catalytic onset shift to more positive potentials (from −1.62 to −1.44 V). Based on equation (1), this reduction occurred at an overpotential of 272 mV.
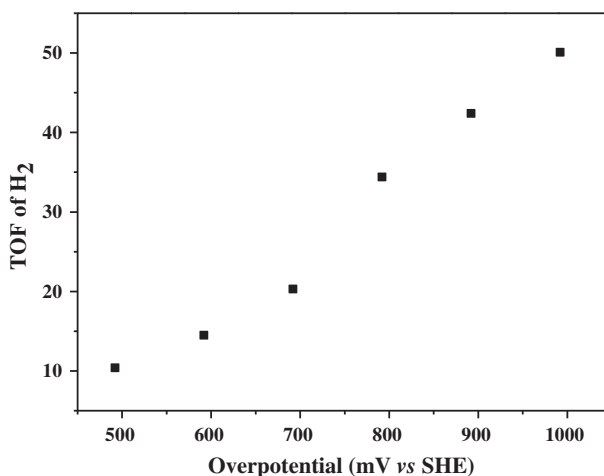

Figure 6. TOF (mol H$_2$/mol catalysts/h) for electrocatalytic hydrogen production by **1** (8.1 μM) under overpotentials *vs.* SHE.

$$E_{HA}^{\ominus} = E_{H}^{\ominus +} - (2.303RT/F)pK_{aHA} \tag{1}$$

A number of control experiments were carried out to verify that **1** is responsible for the catalysis. In particular, acetic acid, the free ligand, CuCl$_2$, and the mixture of the free ligand and CuCl$_2$ were each measured under identical conditions. As can be seen in figures S2–S5, the catalytic competency achieved with **1** is not matched by just ligand, CuCl$_2$, or the mixture of the free ligand and CuCl$_2$, as might arise from dissociation of the ligand, nor can it be accomplished with the ligand bound to a redox-inactive metal. Thus, a combination of the redox-active Cu ion and the ligand is essential for catalytic activity.

Further evidence for the electro-catalytic activity was obtained by bulk electrolysis of a DMF solution of **1** (8.1 μM) with acetic acid (50 mM) at variable applied potentials using a glassy carbon plate electrode in a double-compartment cell. A series of applied potentials
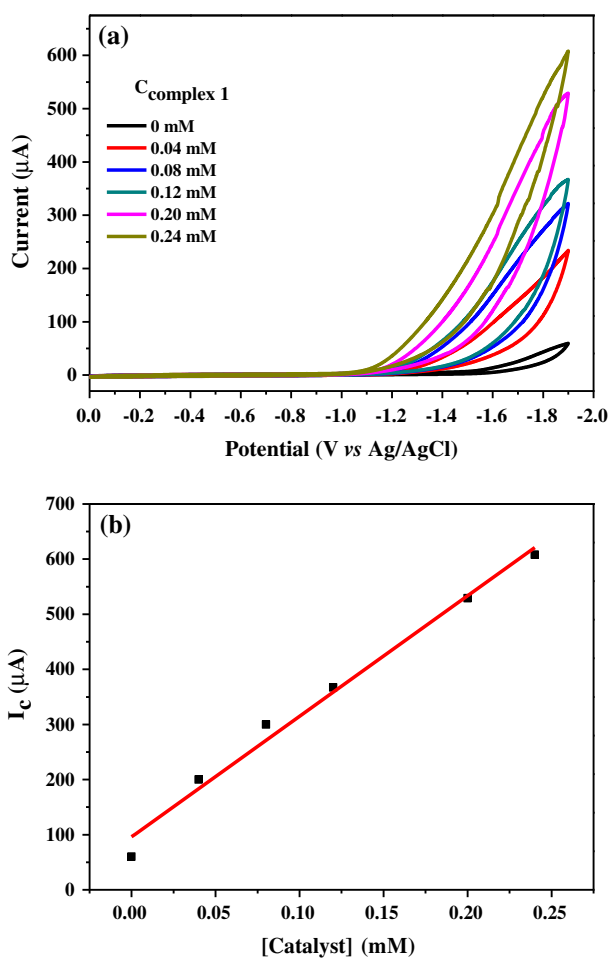

Figure 7.   (a) Cyclic voltammograms of **1** at various concentrations (pH 7.0, scan rate: 100 mV s^{-1}). (b) Plot of catalytic peak current *vs.* concentrations of **1**.

were chosen, corresponding to the electrocatalytic potentials observed in cyclic voltammograms. Figure 5 shows the total charge of bulk electrolysis of **1** in the presence of acid; the charge significantly increased when the applied potential was added. Assuming every catalyst molecule was distributed on the electrode surface and every electron was used for the reduction of protons. According to equation (2) [28], we calculated turnover frequency (TOF) for the catalyst reaching a maximum of 50.1 M of hydrogen per mole of catalyst per hour (equation (3) in supplementary material and figure 6),

$$\text{TOF} = \Delta C / (F^* n_1^* n_2^* t) \tag{2}$$

where ΔC is the charge from the catalyst solution during CPE minus the charge from the solution without catalyst during CPE, F is Faraday's constant, n_1 is the moles of electrons
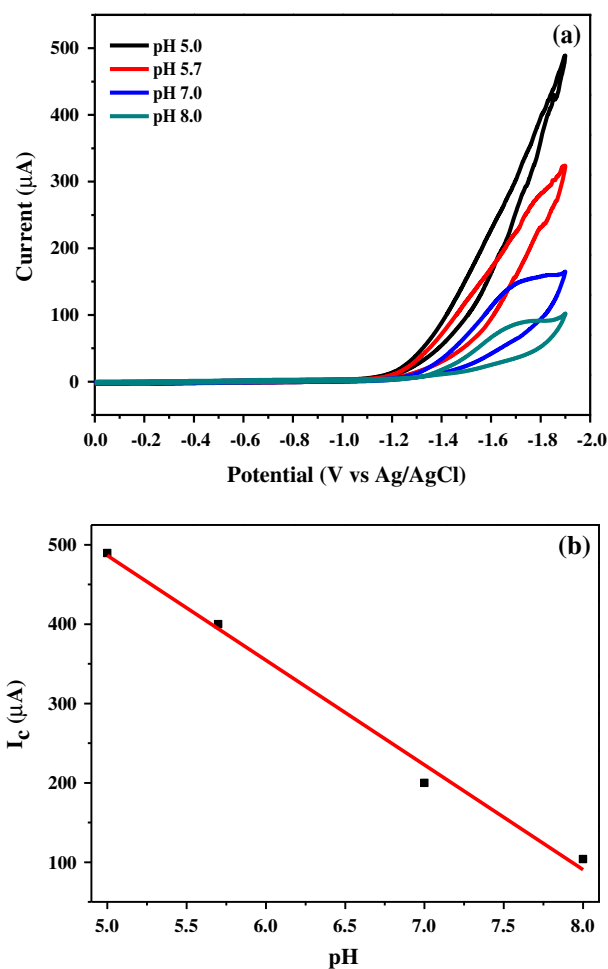
Figure 8.   (a) CVs of **1** showing the variation in catalytic current with pH (scan rate: 100 mV s^{-1}). (b) Catalytic current maximum (i_c) as a function of pH.

required to generate 1 M of H_2, n_2 is the moles of catalyst in solution, and t is the duration of electrolysis.

3.5. *Catalytic hydrogen evolution in aqueous media*

We also tried to explore the catalytic hydrogen evolution in aqueous media, a much more attractive medium for the sustainable generation of hydrogen. CVs were conducted in 0.25 M phosphate buffers at different pH values. As shown in figure 7, in the absence of **1**, a catalytic current was not apparent until a potential of −1.5 V *versus* Ag/AgCl was attained. With addition of **1**, the onset of catalytic current was observed at −1.36 V *versus* Ag/AgCl, and the current strength increased significantly with increasing concentrations of **1** from 0.00 to 0.24 mM. When concentration of **1** reached 0.24 mM, the potential at −1.05 V and current strength did not change obviously. The potential moved positive about 450 mV compared to that in the absence of **1**. Furthermore, it is found that the catalytic current maximum of **1** was also dependent on pH values of buffers (figure 8), indicating this catalyst is functioning in a diffusion-controlled regime and is molecular in nature.

Catalytic hydrogen production can also be achieved with **1** in buffer. Figure 9 shows the total charge of bulk electrolysis of the solution containing **1** at pH 7.0. H_2 production can be observed at pH 7.0. When the applied potential was 1.40 V *versus* Ag/AgCl at pH 7.0, the maximum charge was only 23.8 mC during 2 min of electrolysis in absence of **1**. Under the same conditions, the charge reached 234 mC with addition of **1** (8.1 μM) (figure S6), which was confirmed to be H_2 by GC analysis. The evolved H_2 was analyzed by gas chromatography, figure 10, which gave ~12.8 mL of H_2 over an electrolysis period of 1 h with a Faradaic efficiency of 96% for H_2 (figure 11). TOF for electrocatalytic hydrogen production by **1** is 104.3 (pH 7.0) (equation 4 in supplementary material) moles of hydrogen per mole of catalyst per hour (figure S7).
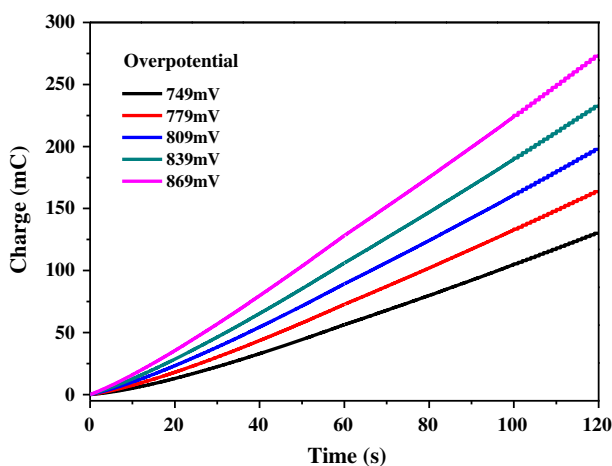

Figure 9. Charge buildup of **1** (8.1 μM) *vs.* applied potentials at various pH values. All data have been deducted blank.
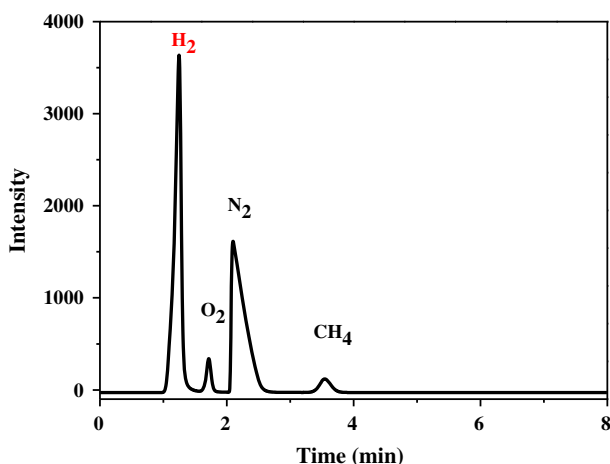
Figure 10.   GC traces after a 1-h CPE at 839 mV *vs.* SHE of 8.1 μM **1** in 0.25 M phosphate buffer, pH 7.0. A standard of CH_4 was added for calibration purposes.
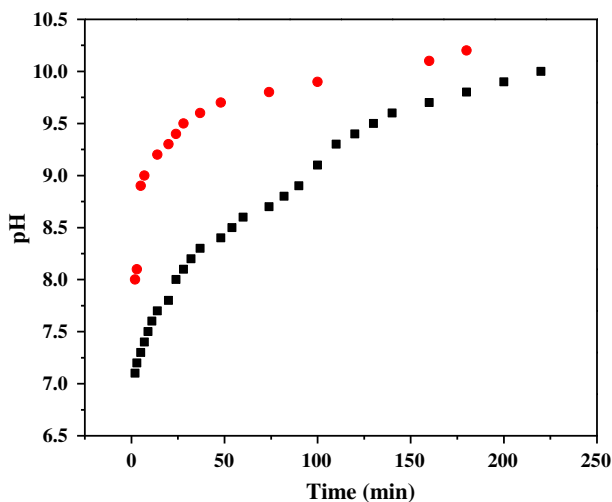

Figure 11.   Practical (red) and theoretical (black) pH changes assuming a 100% Faradaic efficiency of **1** during electrolysis (The theoretical pH change over time can be calculated by the equation $pH = 14 + 1\,g\frac{\sum It}{FV}$ where I = current (A), t = time (s), F = Faraday constant (96,485 CM^{-1}), V = solution volume (0.05 L)) (see http://dx.doi.org/10.1080/00958972.2014.998657 for color version).

4. Conclusion

We have constructed a copper complex, **1**. Electrochemical studies show that **1** can generate dihydrogen from acetic acid and from water. This discovery has established a new chemical paradigm for creating reduction catalysts that are highly active and robust in both organic and aqueous media. Ongoing efforts are focused on modifying ligands and related complexes to further facilitate new functional studies, especially emphasis on chemistry relevant to sustainable energy cycles.

Supporting information

CCDC 661639 contains the supplementary crystallographic data for this paper. This data can be obtained free of charge via http://www.ccdc.cam.ac.uk/conts/retrieving.html, or from the Cambridge Crystallographic Data Center, 12 Union Road, Cambridge CB2 1EZ, UK; Fax: (+44) 1223 336 033; or E-mail: deposit@ccdc.cam.ac.uk.

Funding

References

[1] J.A. Turner. *Science*, **305**, 972 (2004).
[2] T.R. Cook, D.K. Dogutan, S.Y. Reece, Y. Surendranath, T.S. Teets, D.G. Nocera. *Chem. Rev.*, **110**, 6474 (2010).
[3] P.D. Tran, V. Artero, M. Fontecave. *Energy Environ. Sci.*, **3**, 727 (2010).
[4] J.C. Fontecilla-Camps, A. Volbeda, C. Cavazza, Y. Nicolet. *Chem. Rev.*, **107**, 4273 (2007).
[5] P.M. Vignais, B. Billoud. *Chem. Rev.*, **107**, 4206 (2007).
[6] C.J. Pickett, C. Tard. *Chem. Rev.*, **109**, 2245 (2009).
[7] T. Goris, A.F. Wait, M. Saggu, J. Fritsch, N. Heidary, M. Stein, I. Zebger, F. Lendzian, F.A. Armstrong, B. Friedrich, O. Lenz. *Nat. Chem. Biol.*, **7**, 310 (2011).
[8] B.J. Fisher, R. Eisenberg. *J. Am. Chem. Soc.*, **102**, 7361 (1980).
[9] M.L. Helm, M.P. Stewart, R.M. Bullock, M.R. DuBois, D.L. DuBois. *Science*, **333**, 863 (2011).
[10] J.P. Cao, T. Fang, L.Z. Fu, L.L. Zhou, S.Z. Zhan. *Int. J. Hydrogen Energy*, **39**, 10980 (2014).
[11] Y. Sun, J.P. Bigi, N.A. Piro, M.L. Tang, J.R. Long, C.J. Chang. *J. Am. Chem. Soc.*, **133**, 9212 (2011).
[12] W.M. Singh, T. Baine, S. Kudo, S. Tian, X.A.N. Ma, H. Zhou. *Angew. Chem. Int. Ed.*, **51**, 5941 (2012).
[13] B.D. Stubbert, J.C. Peters, H.B. Gray. *J. Am. Chem. Soc.*, **133**, 18070 (2011).
[14] A.D. Nguyen, M.D. Rail, M. Shanmugam, J.C. Fettinger, L.A. Berben. *Inorg. Chem.*, **52**, 12847 (2013).
[15] F. Quentel, G. Passard, F. Gloaguen. *Energy Environ. Sci.*, **5**, 7757 (2012).
[16] H.I. Karunadasa, C.J. Chang, J.R. Long. *Nature*, **464**, 1329 (2010).
[17] S.M. Barnett, K.I. Goldberg, J.M. Mayer. *Nat. Chem.*, **4**, 498 (2012).
[18] T. Zhang, C. Wang, S. Liu, J. Wang, W. Lin. *J. Am. Chem. Soc.*, **136**, 273 (2014).
[19] G.M. Sheldrick. *SADABS, Program for Empirical Absorption Correction of Area Detector Data*, University of Göttingen, Göttingen (1996).
[20] G.M. Sheldrick. *SHELXS 97, Program for Crystal Structure Refinement*, University of Göttingen, Göttingen (1997).
[21] R.N. Patel, D.K. Patel, K.K. Shukla, Y. Singh. *J. Coord. Chem.*, **66**, 4131 (2013).
[22] M.-J. Niu, D.-W. Sun, H.-H. Li, Z.-Q. Cao, S.-N. Wang, J.-M. Dou. *J. Coord. Chem.*, **67**, 81 (2014).
[23] A. Elmali, C.T. Zeyrek, Y. Elerman, I. Svoboda. *Acta Crystallogr.*, **C56**, 1302 (2000).
[24] E.C. Lingafelter, G.L. Simmons, B. Morosin, C. Scheringer, C. Freiburg. *Acta Crystallogr.*, **14**, 1222 (1961).
[25] F. Akhtar, M.G.B. Drew. *Acta Crystallogr. Sect. B Struct. Crystallogr. Cryst. Chem.*, **38**, 1149 (1982).
[26] T.N. Sorrell. *Tetrahedron*, **45**, 3 (1989).
[27] C. Karthick, P. Gurumoorthy, M.A. Imran Musthafa, R. Lakra, P.S. Korrapati, A.K. Rahiman. *J. Coord. Chem.*, **67**, 1794 (2014).
[28] H.I. Karunadasa, E. Montalvo, Y. Sun, M. Majda, J.R. Long, C.J. Chang. *Science*, **335**, 698 (2012).